Biomech Model Mechanobiol (2011) 10:689–699
DOI 10.1007/s10237-010-0266-y

ORIGINAL PAPER

Identification of in vivo material and geometric parameters of a human aorta: toward patient-specific modeling of abdominal aortic aneurysm

Shahrokh Zeinali-Davarani · L. Guy Raguin · David A. Vorp · Seungik Baek

Received: 30 August 2010 / Accepted: 18 October 2010 / Published online: 6 November 2010

Abstract Recent advances in computational modeling of vascular adaptations and the need for their extension to patient-specific modeling have introduced new challenges to the path toward abdominal aortic aneurysm modeling. First, the fundamental assumption in adaptation models, namely the existence of vascular homeostasis in normal vessels, is not easy to implement in a vessel model built from medical images. Second, subjecting the vessel wall model to the normal pressure often makes the configuration deviate from the original geometry obtained from medical images. To address those technical challenges, in this work, we propose a two-step optimization approach; first, we estimate constitutive parameters of a healthy human aorta intrinsic to the material by using biaxial test data and a weighted nonlinear least-squares parameter estimation method; second, we estimate the distributions of wall thickness and anisotropy using a 2-D parameterization of the vessel wall surface and a global approximation scheme integrated within an optimization routine. A direct search method is implemented to solve the optimization problem. The numerical optimization method results in a considerable improvement in both satisfying homeostatic condition and minimizing the deviation of geometry from the original shape based on in vivo images. Finally, the utility of the proposed technique for patient-specific modeling is demonstrated in a simulation of an abdominal aortic aneurysm enlargement.

Keywords Image-based modeling · Inverse optimization · Mechanical homeostasis · Growth and remodeling · Parameter estimation

Dedicated to Professor K.R. Rajagopal on the occasion of his sixtieth birthday.

S. Zeinali-Davarani · S. Baek (✉)
Department of Mechanical Engineering, Michigan State University, 2457 Engineering Building, East Lansing, MI 48824-1226, USA
e-mail: sbaek@egr.msu.edu

L. G. Raguin
Departments of Mechanical Engineering and Radiology, Michigan State University, East Lansing, USA

D. A. Vorp
Departments of Surgery and Bioengineering, Center for Vascular Remodeling and Regeneration, University of Pittsburgh, Pittsburgh, USA

1 Introduction

Abdominal aortic aneurysm (AAA) affects 2 million people in the US alone, and ruptured AAA is one of the leading causes of death. As the population of elderly people grows, the social and economic burden that AAA imposes on the health care system will increase. In order to reduce this public health burden, there are crucial needs for advanced technologies that can provide AAA patients with early detection, patient-specific risk assessment, and safe clinical interventions. Recent advances in medical image-based stress analysis of AAAs and computational simulation of vascular adaptation show a great potential for computational biomechanics to help develop such technologies.

Finite element (FE) analysis based on 3-D computer tomography and nonlinear constitutive models of the vessel enable researchers to estimate wall stress more accurately (Dorfmann et al. 2010; Fillinger et al. 2002; Raghavan et al. 2000; Rissland et al. 2009; Speelman et al. 2007) and, hence, lead to a better prediction of rupture risk than the maximum diameter criterion. However, the rupture potential depends not only on the stress but also on the strength (Vorp and Vande Geest 2005). Estimation of the stress alone may not

provide a reliable estimation of rupture potential. Furthermore, a classical FE analysis yields the stress distribution only for a fixed AAA geometry and does not model the time evolution of AAA.

On the other hand, computational modeling of vascular growth and remodeling (G&R), as an emerging area in biomechanics, provides a computational tool to model the time evolution of vascular diseases and to test multiple hypotheses generated from experimental and clinical studies. For the past decade, several researchers have developed computational models of vascular adaptation during the progression of vascular diseases (Baek et al. 2006, 2007; Figueroa et al. 2009; Kroon and Holzapfel 2009; Watton and Hill 2009). Many of these models have been built upon the theoretical framework of modeling tissue G&R presented by Humphrey and Rajagopal (2002). They introduced a constrained mixture approach focusing on stress-mediated mass production and removal in evolving stressed configurations. They also offered key remarks that are central to guiding the later development of theories of soft tissue G&R. One of the key remarks is that:

> Normal growth and remodeling tends to be a stable dynamical process, one that seeks to optimize structure and function with respect to yet unidentified parameters. In comparison to processes during development, there appear to be genetic and perhaps epigenetic constraints on this optimization process during maturity.

Furthermore, they emphasized a pressing need to identify both a set of optimization parameters and the associated constraints. Most of the previous computational simulations of vascular adaptation, however, have been developed using idealized geometries for which the identification of homogeneous parameters does not pose a problem. Our recent work suggested that implementing the image-based arterial G&R models based on constrained mixture approach requires an optimization technique to furnish the blood vessel with an optimal structure in normal G&R (Zeinali-Davarani et al. 2010).

In the present study, we address two technical challenges associated with patient-specific modeling of AAA evolution and propose possible solutions. First, as stated earlier, theory of G&R is based on a key assumption, the existence of mechanical homeostasis (Humphrey 2008; Kassab 2008), whereas it is difficult to prescribe the in vivo parameters such that the assumption of a homeostatic state is satisfied at every point in the vessel wall model. For an idealized model, where the blood vessel is assumed to be an ideal thin hollow cylinder, the in vivo material properties are typically assumed to be uniform over the domain. When a medical image-based geometric model is used, however, it is not a trivial task to prescribe the distribution of material and structural parameters such as thickness and fiber orientations.

Second, another difficulty associated with using an image-based model stems from the fact that the in vivo image is obtained under the pressure and the stress-free configuration is not available. Hence, it is difficult to maintain the original patient-specific model in a computational simulation under the in vivo pressure. Inverse elastostatic methods have been pursued to estimate the stress-free state from a pre-deformed in vivo geometry (Lu et al. 2008; Zhou et al. 2010). Others have used a Lagrangian–Eulerian formulation or prescribed numerically estimated material parameters to obtain the meaningful prestressed state (Gee et al. 2009, 2010; Zeinali-Davarani et al. 2010).

In this work, we develop an inverse optimization method to estimate in vivo material parameters for a human aorta using a two-step process. First, we estimate the constitutive parameters intrinsic to the material by fitting the ex vivo biaxial mechanical test data of a healthy human aorta. Second, we solve an optimization problem to estimate the distributions of the wall thickness and anisotropy such that the homeostasis is maintained, while the geometry deviates minimally from the in vivo configuration. Eventually, in order to illustrate the utility of the proposed method in computational G&R simulations, the estimated material parameters as well as the distributions of wall thickness and anisotropy are prescribed and an AAA is simulated by introducing spatial elastin degradation to the vessel wall model.

2 Method

2.1 Estimation of material constitutive parameters

As the first step, we estimate the constitutive parameters by fitting biaxial mechanical test data of a healthy human aorta (Vande Geest et al. 2004, 2006). Here, we briefly explain the kinematics and constitutive relations.

Figure 1 shows a schematic drawing for the kinematics of deformation related to a biaxial test of a healthy aorta. The in vivo configuration of a healthy aorta is assumed to be the prestressed reference configuration κ_R, whereas κ_I represents the intermediate configuration of the square-cut sample under the traction-free condition. The deformation gradient $\mathbf{F}^R$ corresponds to the mapping from κ_R to κ_I. It is assumed that there is no active tone presented during the biaxial test. The deformation gradient $\mathbf{F}^I$ corresponds to the mapping from κ_I to the deformed configuration during the biaxial test, resulting in $\mathbf{F} = \mathbf{F}^I\mathbf{F}^R$. Assuming incompressibility in an ideal geometry,

$$\mathbf{F}^R = \mathrm{diag}\left\{F_1^R, F_2^R, \frac{1}{F_1^R F_2^R}\right\}$$

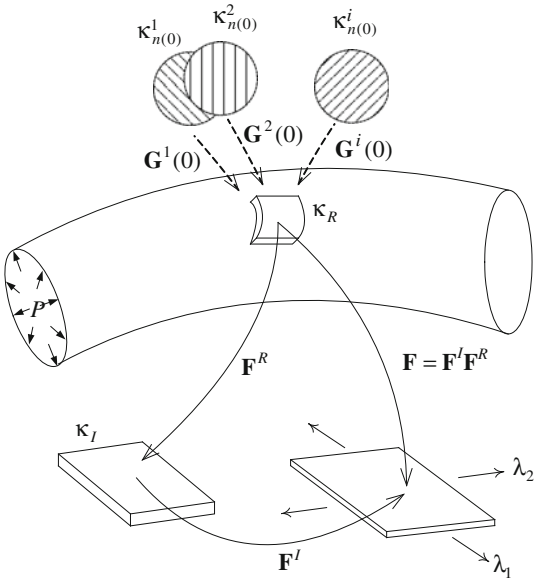

Fig. 1 Kinematics of the deformation associated with biaxial mechanical test and the corresponding deformation gradients. λ_1 and λ_2 are stretches in circumferential and axial directions during the biaxial test

$$\mathbf{F}^I = \text{diag}\left\{\lambda_1, \lambda_2, \frac{1}{\lambda_1\lambda_2}\right\}, \tag{1}$$

where $F^R_1, F^R_2 < 1.0$ and $\lambda_1, \lambda_2 > 1.0$.

The arterial wall is assumed to be a mixture of constituents 'i' such as elastin ($i = e$), multiple collagen families ($i = 1, \ldots, k, \ldots, 4$), and smooth muscle ($i = m$). The strain energy of the mixture per unit reference area is $w = \sum_i w^i = w^e + \sum_k w^k + w^m + w^m_{act}$, and the membrane stress is given as (Baek et al. 2006; Humphrey 2002)

$$\mathbf{T} = \frac{2}{J}\mathbf{F}\frac{\partial w}{\partial \mathbf{C}}\mathbf{F}^T, \tag{2}$$

where J is a determinant of the 2-D deformation gradient $\mathbf{F}$ and $\mathbf{C} = \mathbf{F}^T\mathbf{F}$. The stretches of the smooth muscle (SM) and collagen fiber 'k' from their natural (stress-free) configuration to the current configuration are given as

$$\lambda^k_n = G^c_h \lambda^k \tag{3}$$

$$\lambda^m_n = G^m_h \lambda_1, \tag{4}$$

where G^m_h and G^c_h are homeostatic stretches of SM and collagen. We define a new tensor

$$\tilde{\mathbf{G}}^e = \text{diag}\left\{G^e_1, G^e_2, \frac{1}{G^e_1 G^e_2}\right\}, \tag{5}$$

which represents a mapping from the natural configuration of elastin to the reference configuration such that,

$$\mathbf{F}^e_n = \mathbf{F}\tilde{\mathbf{G}}^e, \quad \mathbf{C}^e_n = \mathbf{F}^{e\,T}_n \mathbf{F}^e_n = \left[\tilde{\mathbf{G}}^e\right]^T \mathbf{C}\tilde{\mathbf{G}}^e. \tag{6}$$

Strain energies of the constituents i per unit reference area, w^i, are given as

$$w^e\left(\mathbf{C}^e_n(t)\right) = M^e \frac{c_1}{2}\left(C^e_{n[11]} + C^e_{n[22]} + \frac{1}{C^e_{n[11]}C^e_{n[22]} - {C^e_{n[12]}}^2} - 3\right) \tag{7}$$

$$w^k\left(\lambda^k_n\right) = M^k \frac{c_2}{4c_3}\left\{\exp\left[c_3\left(\left(\lambda^k_n\right)^2 - 1\right)^2\right] - 1\right\} \tag{8}$$

$$w^m\left(\lambda^m_n\right) = M^m \frac{c_4}{4c_5}\left\{\exp\left[c_5\left(\left(\lambda^m_n\right)^2 - 1\right)^2\right] - 1\right\} \tag{9}$$

$$w^m_{act} = M^m \frac{S}{\rho}\left\{\lambda_1 + \frac{1}{3}\frac{(\lambda_M - \lambda_1)^3}{(\lambda_M - \lambda_o)^2}\right\}, \tag{10}$$

where M^i is the mass per unit reference area for the constituent i. $C^e_{n[11]}$, $C^e_{n[22]}$ and $C^e_{n[12]}$ are components of $\mathbf{C}^e_n$. λ_M and λ_o are stretches at which the SM contraction is maximum and at which active force generation ceases, S is the stress at the maximum contraction of SM.

Components of $\mathbf{F}^R$ are obtained by considering stress as a function of deformation gradient, i.e. $\mathbf{T} = \hat{\mathbf{T}}(\mathbf{F})$, and assuming that membrane stresses vanish at $\mathbf{F} = \mathbf{F}^R$ such that

$$\hat{\mathbf{T}}\left(\mathbf{F}^R\right) = \mathbf{0}. \tag{11}$$

Based on literature, we prescribe some of the parameters as following (He and Roach 1994; Holzapfel et al. 2002; Menashi et al. 1987; Zeinali-Davarani et al. 2010):

$$\begin{aligned} &\nu^e = 0.2, \quad \nu^m = 0.2, \\ &\nu^k = [0.1, 0.1, 0.4, 0.4](1 - \nu^e - \nu^m), \\ &\alpha^k = [0°, 90°, 45°, 135°], \end{aligned} \tag{12}$$

where ν^i is the mass fraction of the constituent i for the normal artery and α^k is the orientation of the kth collagen fiber family. Collagen fibers are significantly less stiff under compression, and we assume a different value of $c_2^{(comp)}$ in compression. Parameters $[c_1, c_2, c_3, c_4, c_5, G^e_1, G^e_2, G^c_h, G^m_h]$ and $c_2^{(comp)}$ are assumed to be unknown and to be estimated by the parameter estimation.

Best-fit parameters are estimated using the weighted nonlinear least-squares method described by Zeinali-Davarani et al. (2009). Figure 2 shows the biaxial test data of a healthy human aorta (Vande Geest et al. 2004, 2006) as well as the fitted values using the estimated parameters. The best-fit values of the estimated parameters are given in Table 1.

Although the existence of mechanical homeostasis in vasculature is generally accepted, the theoretical formulation that describes vascular adaptations in response to diverse stimuli is not completely established yet. Nevertheless, we utilize scalar measures of stress as the intramural stress of

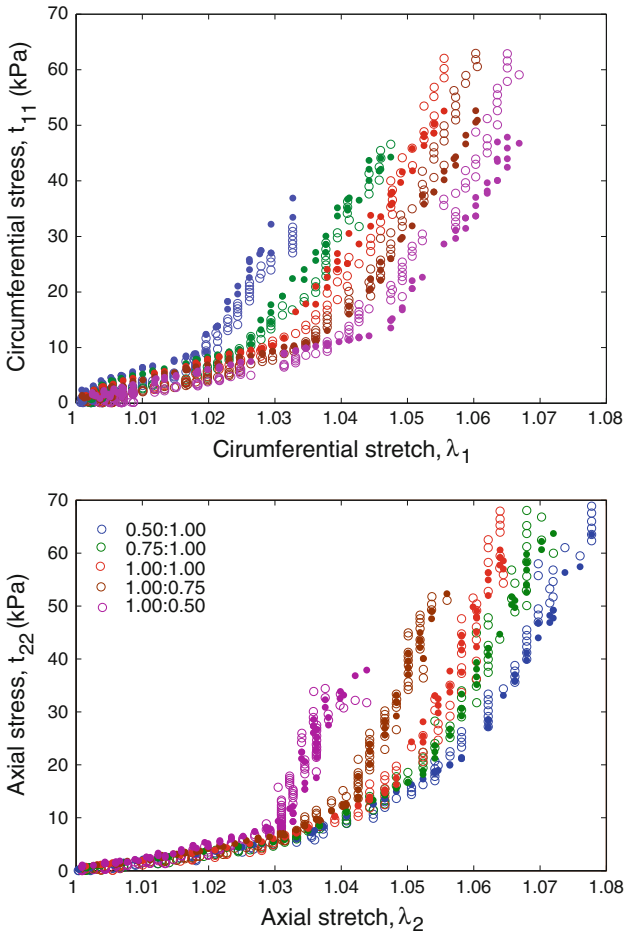

Fig. 2 Stress versus stretch plots in circumferential (*top*) and axial (*bottom*) directions. Data (*circles*) and fitted values (*dots*) using the estimated parameters. Each set of data (*different colors*) corresponds to a different ratios of tensions applied in both directions during a biaxial test

constituents (Baek et al. 2006; Figueroa et al. 2009; Zeinali-Davarani et al. 2010)

$$\sigma^k = \left\| \left(\sum_k \nu^k \boldsymbol{\sigma}^k \right) \mathbf{n}^k \right\|, \quad \sigma^m = \left\| \boldsymbol{\sigma}^m \mathbf{n}^m \right\|, \tag{13}$$

where $\boldsymbol{\sigma}^k$ and $\boldsymbol{\sigma}^m$ are the stresses of the kth collagen fiber and SM, respectively, and $\mathbf{n}^k$ and $\mathbf{n}^m$ are unit vectors in the directions of the kth collagen fiber and SM. Using the estimated parameters, the homeostatic stress of collagen and SM are then calculated as $\sigma_h^c = 143\,\text{kPa}$ and $\sigma_h^m = 81\,\text{kPa}$. The prescribed parameters associated with SM tone are $\lambda_M = 1.4$, $\lambda_0 = 0.8$ and $S = 54\,\text{kPa}$ (Zeinali-Davarani et al. 2010).

2.2 Inverse optimization problem statement

As the next step, we estimate the distributions of wall thickness and material anisotropy using an inverse optimization method where both the deviation of geometry from the in vivo configuration and the deviation of stress from the homeostatic value are minimized. Then, the objective function to minimize is

$$W = \frac{\int_\Omega \left\| \mathbf{x}\left(h, \alpha^k\right) - \mathbf{X}_{image} \right\|^2 \mathrm{d}A}{\int_\Omega \left\| \mathbf{X}_{image} - \bar{\mathbf{X}} \right\|^2 \mathrm{d}A} + \xi \sum_i \frac{\nu^i \int_\Omega \left(\sigma^i\left(h, \alpha^k\right) - \sigma_h^i\right)^2 \mathrm{d}A}{\int_\Omega \left(\sigma_h^i\right)^2 \mathrm{d}A} \tag{14}$$

where $i = m, 1, \ldots, k$ and $\mathbf{x}$ is the FE solution for position vector and $\mathbf{X}_{image}$ is the position vector from medical image and $\bar{\mathbf{X}}$ is the geometric center of the artery. σ^i is a scalar measure of stress in the direction of the constituent i obtained from the FE analysis (See Zeinali-Davarani et al. (2010) for detailed explanation of the image-based FE model of the arterial wall). σ_h^i and ν^i are the homeostatic stress and mass fraction assumed for the constituent i. (h, α^k) are the unknown wall thickness and anisotropy, i.e. orientation of the collagen fiber k. The objective function is composed of two additive terms and a weight parameter ξ; first term is related to the deviation of geometry (named "$\mathcal{GD}$" hereafter) and the second term is related to the deviation of stress (named "$\mathcal{SD}$" hereafter).

However, solving this optimization problem for the thickness and anisotropy at all nodal points of the FE model is not practical, even if possible. Thickness and anisotropy distributions can be approximated with a smaller (I) number of variables with associated base functions, independent from the FE mesh as

$$\begin{aligned} h(x, y, z) &= \sum_{j=1}^{I} \left\{ \beta_j^h \phi_j(x, y, z) \right\} \quad (x, y, z) \in \Omega \\ \alpha^k(x, y, z) &= \sum_{j=1}^{I} \left\{ \beta_j^k \psi_j(x, y, z) \right\} \quad (x, y, z) \in \Omega, \end{aligned} \tag{15}$$

where $\left(\beta_j^h, \beta_j^k\right)$ are variables for thickness and anisotropy associated with the approximation point j. $\phi_j(x, y, z)$ and $\psi_j(x, y, z)$ are basis/approximation functions defined on the computational domain Ω. The objective function then can

Table 1 Estimated constitutive parameters for each constituent from the parameter estimation, used for G&R simulations

Elastin:	$c_1 = 50.6\,\text{Pa/kg}$, $G_1^e = 1.22$, $G_2^e = 1.23$
Collagen:	$c_2 = 3195\,\text{Pa/kg}$, $c_2^{(comp)} = 0.1c_2$, $c_3 = 25.0$, $G_h^c = 1.034$
SM:	$c_4 = 16.45\,\text{Pa/kg}$, $c_5 = 14.14$, $G_h^m = 1.165$

be rewritten with respect to the new design variables as

$$W = \frac{\int_\Omega \left\| \mathbf{x}\left(\beta_j^h, \beta_j^k\right) - \mathbf{X}_{image} \right\|^2 \mathrm{d}A}{\int_\Omega \left\| \mathbf{X}_{image} - \bar{\mathbf{X}} \right\|^2 \mathrm{d}A} + \xi \sum_i \frac{v^i \int_\Omega \left(\sigma^i\left(\beta_j^h, \beta_j^k\right) - \sigma_h^i\right)^2 \mathrm{d}A}{\int_\Omega \left(\sigma_h^i\right)^2 \mathrm{d}A}. \tag{16}$$

To facilitate the approximation in (15), the computational domain (the mid-surface of the vessel wall) can be parameterized by two spatial variables (s, θ) where s and θ represent, respectively, the longitudinal distance and azimuthal position on the arterial wall (see Appendix for details of this mapping). Then, Eq. (15) can be rewritten as

$$\begin{aligned} h(s,\theta) &= \sum_{j=1}^{I} \left\{ \beta_j^h \phi_j(s,\theta) \right\} \\ \alpha^k(s,\theta) &= \sum_{j=1}^{I} \left\{ \beta_j^k \psi_j(s,\theta) \right\}. \end{aligned} \tag{17}$$

Toward solving the optimization problem (Eq. 16), we use initial values of $\left(\beta_j^h, \beta_j^k\right)$ that approximate a homogenous field of thickness and anisotropy $\left(h_0, \alpha_0^k\right)$. That is, the initial values are obtained by solving the following sets of least-squares optimizations

$$S^h = \sum_{e=1}^{N_e} \left(\sum_{j=1}^{I} \beta_j^h \phi_j(s_e,\theta_e) - h_0 \right)^2 \tag{18}$$

$$S^k = \sum_{e=1}^{N_e} \left(\sum_{j=1}^{I} \beta_j^k \psi_j(s_e,\theta_e) - \alpha_0^k \right)^2, \tag{19}$$

where N_e and I are the number of elements and approximation points, respectively.

2.3 Global approximation approach

For an approximation, a product of Legendre polynomials and periodic functions, respectively, for longitudinal and azimuthal directions is used

$$h(s,\theta) = \sum_{m,n=0}^{m=M-1,n=N-1} \beta_{mn}^h P_m(s) F_n(\theta) \tag{20}$$

$$\alpha^k(s,\theta) = \sum_{m,n=0}^{m=M-1,n=N-1} \beta_{mn}^k P_m(s) F_n(\theta), \tag{21}$$

where M and N are, respectively, the total number of Legendre polynomials and periodic functions (i.e. $I = M \times N$). $P_m(s)$ is a univariate Legendre polynomials of order m such that $P_0(s) = 1$, $P_1(s) = s$ and

$$P_{m+1}(s) = s\left(\frac{2m+1}{m+1}\right) P_m(s) - \left(\frac{m}{m+1}\right) P_{m-1}(s). \tag{22}$$

Also, we consider $F_0(\theta) = 1$ and

$$\begin{aligned} F_{2n-1} &= \sin(n\theta) \\ F_{2n} &= \cos(n\theta). \end{aligned} \tag{23}$$

2.4 Optimization algorithm

We employ the Nelder–Mead Simplex method (Lagarias et al. 1998; Nelder and Mead 1965) for the optimization. As a direct search method, it does not require gradients of the function, which is desirable in applications where the calculation of gradients of the function is computationally expensive. Another feature of the Nelder–Mead Simplex method is the fast reduction in the objective function after the first few iterations (Wright 1996). A stopping criterion is chosen based on both the relative size of the simplex and function values at vertices of the simplex as (Torczon 1989):

$$\frac{1}{\Delta} \max_{1 \le j \le I} \left\| v_j^k - v_0^k \right\| < \delta \tag{24}$$

$$W\left(v_I^k\right) - W\left(v_0^k\right) < \epsilon, \tag{25}$$

where v_j^k is the jth vertex of the simplex and a vector comprised of all optimization variables at kth iteration. v_0^k and v_I^k are the "best" and "worst" vertices of the simplex at kth iteration and $\Delta = \max\left(1, \left\| v_0^k \right\|\right)$.

3 Results

A 3-D model of an aorta was reconstructed from MRI data of a healthy subject, and a computational mesh for the arterial wall was generated using triangular elements (Sheidaei et al. 2010). As a parametric study, we first investigate the effect of variation of the weight parameter ξ. Figure 3 shows the $\mathcal{GD}$ and $\mathcal{SD}$ corresponding to minimum values of the objective function obtained with different values of ξ and using two different combinations of Legendre polynomials and periodic functions ($M = 3, N = 3$) and ($M = 6, N = 5$).

In both cases, small values of ξ puts more weight on $\mathcal{GD}$ to minimize the objective function and increasing ξ shifts the weight toward $\mathcal{SD}$. The tradeoff choice according to both cases appears to be $\xi = 0.01$ such that both parts can be minimized at the same time (Fig. 3).

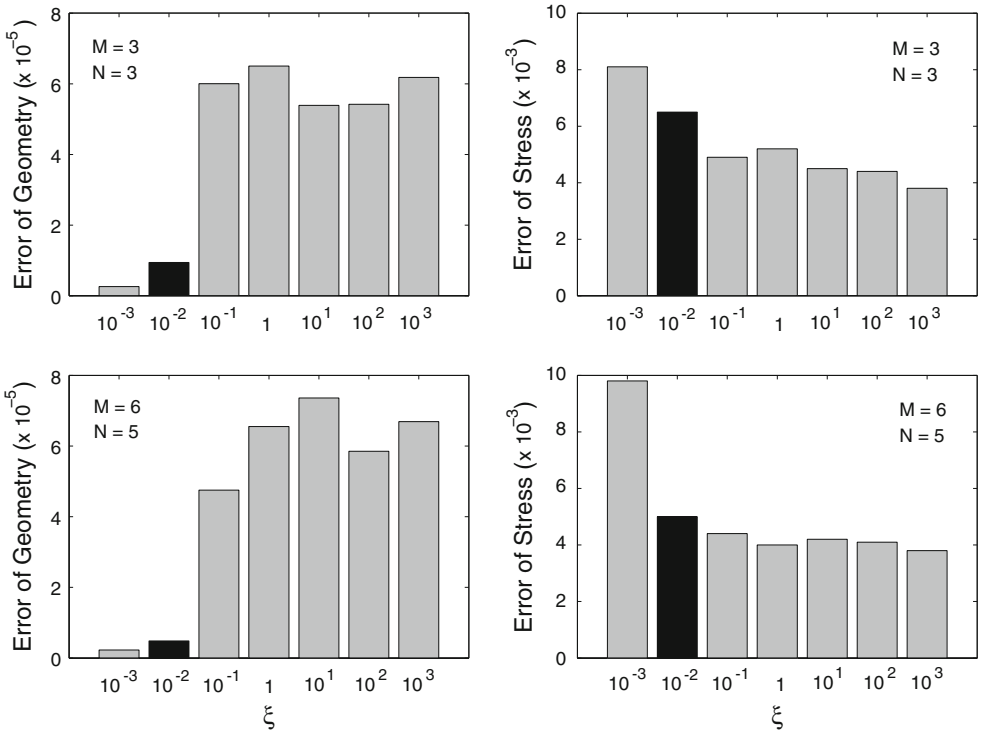

Fig. 3 The effect of variation of the parameter ξ on both $\mathcal{GD}$ and $\mathcal{SD}$ using ($M = 3$, $N = 3$; *top*) and ($M = 6$, $N = 5$; *bottom*)

3.1 Finding the optimal distributions of thickness and anisotropy

We choose 6 Legendre polynomials ($M = 6$) and 3 periodic functions ($N = 3$) for the approximation assuming $\xi = 0.01$. This constitutes 18 variables ($I = 18$) for thickness and anisotropy, including a total of 36 variables into the optimization process. Note that fibers oriented in circumferential and axial directions are considered fixed and only helical fibers orientations are assumed to be changing ($\alpha^3 = -\alpha^4$). Least-squares estimation of variables associated with a homogenous field of thickness and anisotropy (e.g. 0.8 mm for thickness and 50.0° for anisotropy) yielded estimates such as $\beta^h_{00} = 0.8$, $\beta^k_{00} = 50.0$ and 0 for all other parameters. Figure 4 illustrates the convergence history of the objective function as well as its compartments, $\mathcal{GD}$ and $\mathcal{SD}$, until the stopping criterion is met. A fast decrease in the objective function during the first 100 iterations is noticeable, which is accompanied by sharp decreases in $\mathcal{GD}$ and $\mathcal{SD}$. The appearance of the plateau regions is associated with the iterations during which searching the space has not led to a new minimum.

For the sake of comparison, we prescribe the distributions of thickness using the same method employed by Zeinali-Davarani et al. (2010) and compare the results with the current method. Figure 5 contrasts the deviation from the in vivo/image geometry ($||\mathbf{x} - \mathbf{X}_{image}||$) using both methods. A

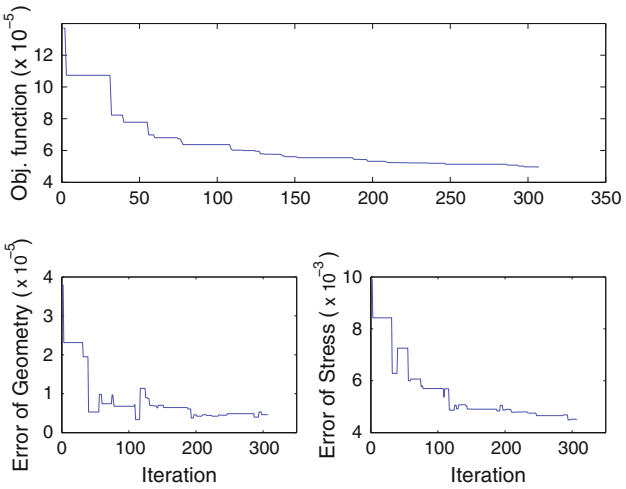

Fig. 4 Changes in the objective function and its associated compartments versus optimization iterations using 36 variables (18 variables for approximating thickness and 18 variables for approximating fiber orientation) considering $\xi = 0.01$

significant decrease in the maximum deviation (about 70%) is achieved using the optimization approach.

The normalized deviation of stress from the homeostatic value $\left(\left(\sigma^k - \sigma^k_h\right)/\sigma^k_h\right)$ in the direction of helical fiber families ($k = 3, 4$) using both methods are shown in Figs. 6 and 7. For fiber families of both helical directions, the maximum deviations of stress from the homeostatic value are significantly decreased by 70% using the optimization method.

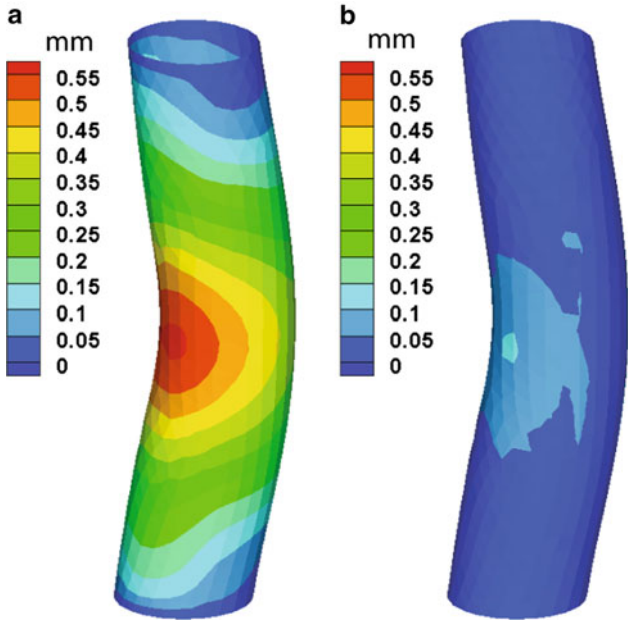

Fig. 5 Deviation of the geometry from the in vivo geometry without (**a**), and with (**b**), optimized distributions of thickness and anisotropy ($||\mathbf{x} - \mathbf{X}_{image}||$)

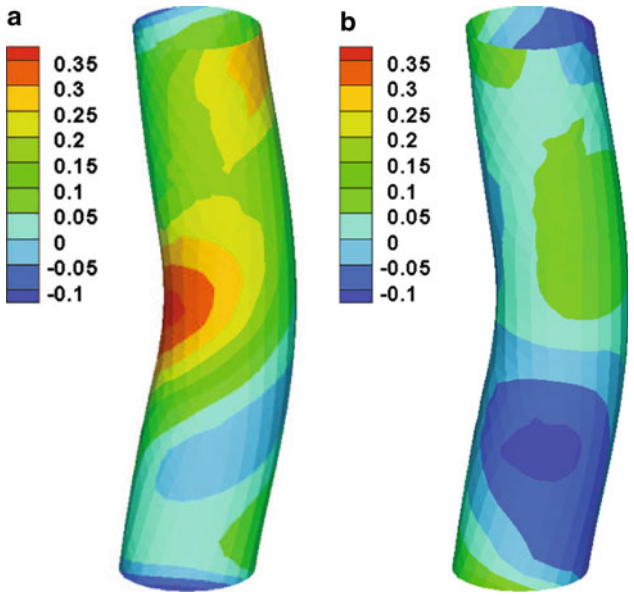

Fig. 6 Deviation of the stress $\left((\sigma^k - \sigma_h^k)\,/\,\sigma_h^k\right)$ from the target homeostatic stress in a helical fiber ($k = 3$) without (**a**), and with (**b**), optimized distributions of thickness and anisotropy

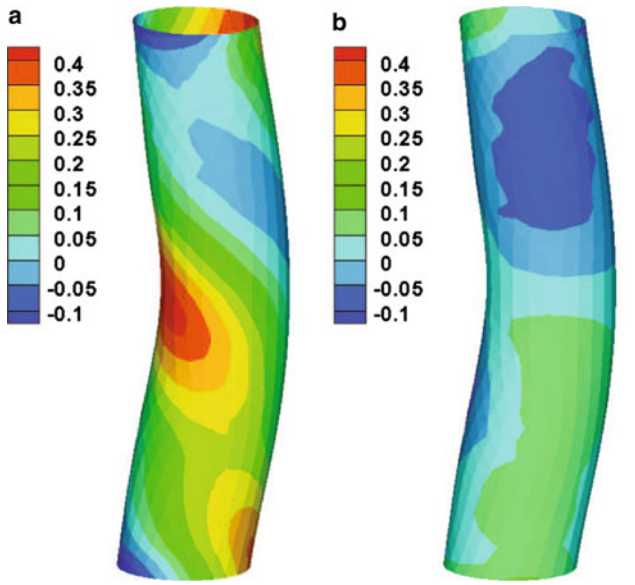

Fig. 7 Deviation of the stress $\left((\sigma^k - \sigma_h^k)\,/\,\sigma_h^k\right)$ from the target homeostatic stress in a helical fiber ($k = 4$) without (**a**), and with (**b**), optimized distributions of thickness and anisotropy

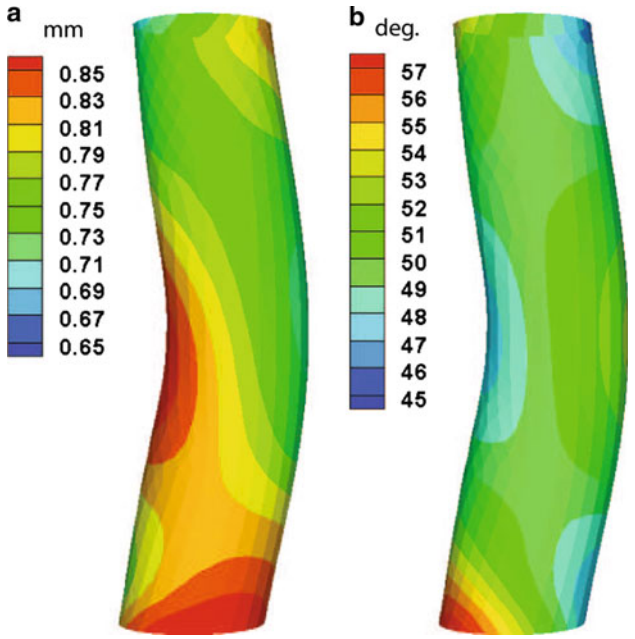

Fig. 8 Distributions of thickness (**a**), and anisotropy (**b**), obtained from the optimization results using $\xi = 0.01$, $M = 6$, and $N = 3$

Figure 8 depicts the distributions of wall thickness and anisotropy obtained by the optimization with $\xi = 0.01$, $M = 6$, and $N = 3$. The resulting spatial variation of anisotropy is not large although thickness considerably varied especially on the convex and concave regions with higher values on the concave side and lower values on the convex side.

3.2 Simulation of AAA enlargement

When the optimal solution to the problem is achieved by the inverse method, AAA simulations are initiated by applying instantaneous elastin degradation with different spatial distribution functions (See Baek et al. (2006); Zeinali-Davarani et al. (2010) for details of the G&R framework and its application to image-based models). Figure 9 shows the spatial

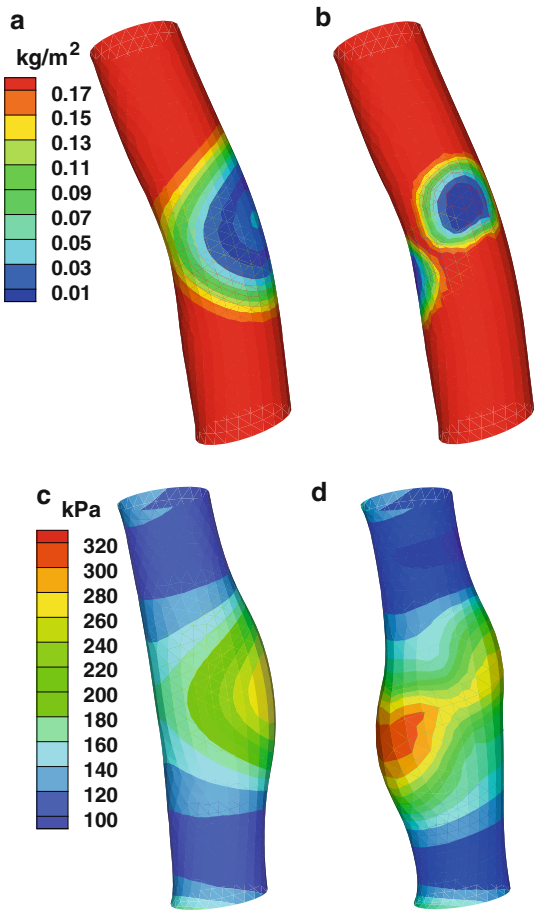

Fig. 9 Distributions of elastin content after applying elastin degradation with different spatial functions (**a**, **b**), and the corresponding distributions of maximum principal stress after 1,700(**c**), and 2,600(**d**) days of G&R

distributions of elastin degradation (a,b) and the resulting distributions of the maximum principal stress after 1,700 (c) and 2,600 (d) days of G&R. Due to the stress-driven G&R, the portions of the wall subject to elastin degradation and higher stress expand. The effect of variation of kinetic parameters that control the stress-mediated G&R has been studied in detail by Zeinali-Davarani et al. (2010).

4 Discussion

The existence of the vascular mechanical homeostasis and the subsequent adaptation in response to mechanical stimuli have been fundamental assumptions in mathematical models of vascular G&R (Baek et al. 2006, 2007; Figueroa et al. 2009; Kroon and Holzapfel 2009; Watton and Hill 2009). There has been a growing interest in using such models on a patient-specific basis (Humphrey and Taylor 2008; Taylor and Humphrey 2009). Toward that goal, image-based arterial geometries have been incorporated into stress-mediated vascular adaptation models (Sheidaei et al. 2010; Zeinali-Davarani et al. 2010). Zeinali-Davarani et al. (2010) utilized the G&R model itself as an optimization tool to drive the mechanical state toward the target homeostatic value before the main G&R simulations begun. This approach, however, alters the in vivo configuration even though it provides a desirable stress distribution. Rather, the present study provides an optimization technique to minimize both deviations from the homeostatic stress and the in vivo configuration simultaneously.

Numerous methods have been presented in order to compensate for the lack of information about stress-free or load-free configurations in patient-specific modeling. Raghavan et al. (2006) used an optimization technique as an approximate method to find the zero-pressure geometry assuming consistency of displacement field patterns. Using an inverse elastostatic method, Lu et al. (2007) were able to determine load-free configuration of an AAA as well as accurate wall tension in a cerebral aneurysm (Lu et al. 2008). Recently, Zhou and Lu (2009) used the same inverse technique to estimate the open configuration of vessels. In a different approach, Gee et al. (2009, 2010) showed the utility of the "modified updated Lagrangian" method in finding meaningful stress analysis results for complex shapes of aneurysms.

However, all of those studies assumed homogenous distributions of the wall thickness and anisotropy, whereas variation of these parameters can have a great impact on the stress/strain distribution. Instead of finding the load-free configuration, our approach focused on the in vivo configuration and its associated material and geometric parameters of arteries using an inverse optimization method such that the homeostatic condition was restored, while the deviation of geometry from the original in vivo configuration was minimized. In a somewhat similar approach, Kroon and Holzapfel (2008a) estimated the distribution of elastic properties of an inhomogeneous and anisotropic membrane using an inverse optimization method and applied the technique to find material properties of the cerebral aneurysm (Kroon and Holzapfel 2008b). They used an element partition method for the robust estimation of properties over the domain. That is, they divided the domain into large sub-domains and performed the optimization for each sub-domain with homogeneous properties. In the next levels of partitioning, they refined each sub-domain while repeating the estimation process with updated initial values. Alternatively, we used a global approximation scheme in order to reduce the number of unknown variables of optimization and to facilitate estimation of the inhomogeneous properties in a global fashion. Increasing the number of approximation variable theoretically improves the objective function even more, but at the cost of more computation time. Deviation of stress from the homeostatic value in both helical directions was dropped by more than 70%, whereas there was no significant reduction in

stress of axial and circumferential fibers (not shown), mainly because of much lower mass fractions assumed in those directions (See Eq. 16). Results of the AAA simulations using the optimal material parameters, wall thickness and anisotropy were generally comparable with Zeinali-Davarani et al. (2010), but more advantageous as the current method reduced the deviation of geometry from the in vivo configuration before the G&R process initiated.

Direct validation of the optimal distributions of the wall thickness and fiber orientations requires more experimental data using animal or human arteries. Nevertheless, the proposed optimization technique provides a useful initialization step, indispensable to patient-specific G&R simulations.

In closing, in this work, we used a scalar measure of stress as a mechanical state governing the mechanosensitive vascular adaptation (Baek et al. 2006). However, it is still controversial what quantity is responsible for the mechanical homeostatic state (stress, strain, material stiffness, or their combination?). We suggest that the proposed inverse method can be used to discriminate among different hypotheses of homeostasis through comparison with experimental data. Such studies may shed light upon the path to the patient-specific modeling of AAA and its clinical interventions.

Acknowledgments This work is supported in part by IRGP grant from Michigan State University (SB) and by NIH grants R01-HL-60670 and R01-HL-79313 (DAV).

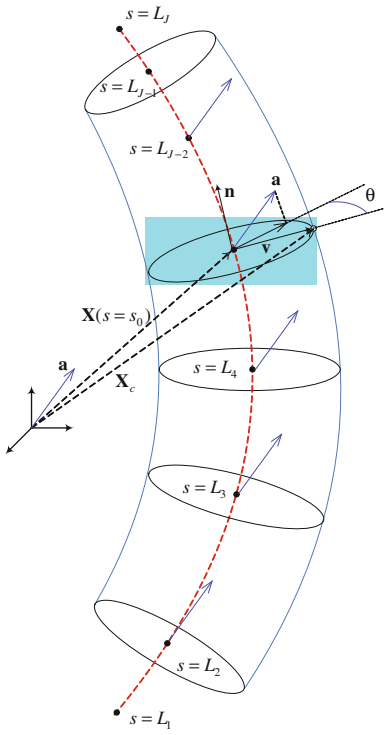

Fig. 10 Geometry of an arbitrary model of the arterial wall with its centerline; Approximation/nodal points with their associated length $s = L_j$ $(j = 1, \ldots, J)$. **a** is an arbitrary vector used in order to find the orientation θ associated with a point (X_c) on the wall

Appendix

A Parameterizing the aortic wall surface with *longitudinal* and *azimuthal* variables

A point on the vessel wall can be parameterized by two variables, one that characterizes its longitudinal position (s) and the other which characterizes its orientation (θ) with respect to a reference direction. To do so, we need to approximate the centerline of the vessel considering some of the points on the centerline as nodal points (Fig. 10) and

$$\mathbf{X}(s) = \sum_i \Phi^i(s)\mathbf{X}^i, \tag{26}$$

where $\mathbf{X}^i$ and Φ^i are the position vector and interpolation function corresponding to the nodal point i on the centerline. $\mathbf{X}$ is the position vector of any point on the centerline as a function of s. A fourth order interpolation function is assumed with the general form of

$$\Phi(s) = c(s-a)^2(s-b)^2. \tag{27}$$

The interpolation functions associated with nodal points $j = 1, \ldots, J$ can be defined as

$$\Phi^1(s) = \frac{(s-L_3)^2(s+L_3)^2}{(L_1-L_3)^2(L_1+L_3)^2} \quad L_1 \le s < L_3 \tag{28}$$

$$\Phi^2(s) = \frac{(s-L_1)^2(s-L_4)^2}{(L_2-L_1)^2(L_2-L_4)^2} \quad L_1 \le s < L_4 \tag{29}$$

$$\Phi^k(s) = \frac{(s-L_{k-2})^2(s-L_{k+2})^2}{(L_k-L_{k-2})^2(L_k-L_{k+2})^2} \quad L_{k-2} \le s < L_{k+2} \tag{30}$$

$$\Phi^{J-1}(s) = \frac{(s-L_{J-3})^2(s-L_J)^2}{(L_{J-1}-L_{J-3})^2(L_{J-1}-L_J)^2} \quad L_{J-3} \le s < L_J \tag{31}$$

$$\Phi^J(s) = \frac{(s-L_{J-2})^2(s+L_{J-2})^2}{(L_J-L_{J-2})^2(L_J+L_{J-2})^2} \quad L_{J-2} \le s < L_J \tag{32}$$

where $k = 3, \ldots, J-2$ and L_j is the value of s at the nodal point j (Fig. 10). These interpolation functions, however, do not satisfy the condition $\sum_{j=1}^{J} \Phi^j(s) = 1$. In order to provide this condition, we need to normalize interpolation functions as

$$\hat{\Phi}^i(s) = \frac{\Phi^i(s)}{\sum_{j=1}^{J} \Phi^j(s)}. \tag{33}$$

Now, using the interpolation in (26), we can find the parameter s associated with any point on the artery, e.g. center point of a triangular element on the surface ($\mathbf{X}_c$). That is, for a given point on the aortic wall, the variable s is calculated by minimizing the distance from the point on the wall to the centerline ($||\mathbf{X}(s) - \mathbf{X}_c||$). The function to be minimized is given as

$$\mathrm{d}(s) = \left(\sum_i \hat{\Phi}^i(s)x^i - x_c\right)^2 + \left(\sum_i \hat{\Phi}^i(s)y^i - y_c\right)^2 + \left(\sum_i \hat{\Phi}^i(s)z^i - z_c\right)^2. \tag{34}$$

Minimizing $\mathrm{d}(s)$ with respect to s results in

$$\frac{\partial \mathrm{d}(s)}{\partial s} = 2\left(\sum_i \hat{\Phi}^i(s)x^i - x_c\right)\sum_i \hat{\Phi}^i_{,s}x^i + 2\left(\sum_i \hat{\Phi}^i(s)y^i - y_c\right)\sum_i \hat{\Phi}^i_{,s}y^i + 2\left(\sum_i \hat{\Phi}^i(s)z^i - z_c\right)\sum_i \hat{\Phi}^i_{,s}z^i = 0. \tag{35}$$

Numerical solution of the nonlinear Eq. (35) is obtained using Newton–Raphson method which also requires the second derivative of the function. The iterative scheme for the Newton–Raphson is formulated as

$$s^{n+1} = s^n - \frac{\frac{\partial \mathrm{d}(s)}{\partial s}|_{s=s^n}}{\frac{\partial^2 \mathrm{d}(s)}{\partial s^2}|_{s=s^n}}. \tag{36}$$

This is repeated for any other point of interest on the wall in order to find the corresponding value of s. If s_0 is the solution associated with a center point of an element (Fig. 10), the vector $\mathbf{v}$ connecting the point on the centerline at $s = s_0$ ($\mathbf{X}(s = s_0)$) and the center point of the element is given as

$$\mathbf{v} = \mathbf{X}_c - \sum_i \hat{\Phi}^i(s_0)\mathbf{X}^i. \tag{37}$$

The normalized vector $\mathbf{n}$ tangent to the centerline at $s = s_0$ is then given by

$$\mathbf{n} = \frac{\frac{\partial \mathbf{X}(s)}{\partial s}|_{s=s_0}}{\left\|\frac{\partial \mathbf{X}(s)}{\partial s}|_{s=s_0}\right\|} \quad \text{where} \quad \frac{\partial \mathbf{X}(s)}{\partial s} = \sum_i \hat{\Phi}^i_{,s}\mathbf{X}^i. \tag{38}$$

The vector $\mathbf{n}$ is also a normal vector to the plane of cross-section at $s = s_0$. Projection of an arbitrary vector $\mathbf{a}$ on the plane of cross-section (Fig. 10) can be assumed as the reference direction

$$\mathbf{a}_p = \mathbf{a} - (\mathbf{a} \cdot \mathbf{n})\mathbf{n}. \tag{39}$$

The angle θ between $\mathbf{a}_p$ and $\mathbf{v}$ characterizes the orientation associated with the current point on the wall (i.e. $\mathbf{X}_c$).

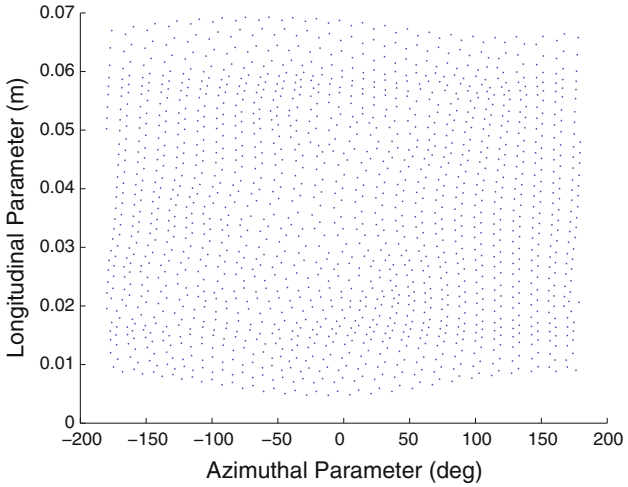

Fig. 11 Geometry of the vessel wall parameterized with longitudinal and azimuthal (s and θ) variables. *Dots* represent center points of all elements on the wall

Figure 11 illustrates the 3-D geometry of the model of aorta mapped in 2-D plane of longitudinal (s) and azimuthal (θ) variables.

References

Baek S, Rajagopal KR, Humphrey JD (2006) A theoretical model of enlarging intracranial fusiform aneurysms. J Biomech Eng 128(1):142–149

Baek S, Valentín A, Humphrey JD (2007) Biochemomechanics of cerebral vasospasm and its resolution: II. Constitutive relations and model simulations. Ann Biomed Eng 35(9):1498–1509

Dorfmann A, Wilson C, Edgar ES, Peatte RA (2010) Evaluating patient-specific abdominal aortic aneurysm wall stress based on flow-induced loading. Biomech Model Mechanobiol 9(2):127–139

Figueroa CA, Baek S, Taylor CA, Humphrey JD (2009) A computational framework for fluid-solid- growth modeling in cardiovascular simulations. Comput Methods Appl Mech Eng 198:3583–3602

Fillinger MF, Raghavan ML, Marra SP, Cronenwell JL, Kennedy FE (2002) In vivo analysis of mechanical wall stress and abdominal aortic aneurysm rupture risk. J Vasc Surg 36(3):589–597

Gee MW, Reeps C, Eckstein HH, Wall WA (2009) Prestressing in finite deformation abdominal aortic aneurysm simulation. J Biomech 42:1732–1739

Gee MW, Forster C, Wall WA (2010) A computational strategy for prestressing patient-specific biomechanical problems under finite deformation. Int J Numer Meth Biomed Engng 26:52–72

He CM, Roach MR (1994) The composition and mechanical properties of abdominal aortic aneurysms. J Vasc Surg 20(1):6–13

Holzapfel GA, Gasser TC, Stadler M (2002) A structural model for the viscoelastic behavior of arterial walls: continuum formulation and finite element analysis. Eur J Mech A Solids 21:441–463

Humphrey JD (2002) Cardiovascular solid mechanics: cells, tissues, and organs. Springer, New York

Humphrey JD (2008) Vascular adaptation and mechanical homeostasis at tissue, cellular, and sub-cellular levels. Cell Biochem Biophys 50:53–78

Humphrey JD, Rajagopal KR (2002) A constrained mixture model for growth and remodeling of soft tissues. Math Models Methods Appl Sci 12:407–430

Humphrey JD, Taylor CA (2008) Intracranial and abdominal aortic aneurysms: similarities, differences, and need for a new class of computational models. Ann Rev Biomed Eng 10:1–26

Kassab GS (2008) Mechanical homeostasis of cardiovascular tissue. In: Artmann GM, Chien S (eds) Bioengineering in cell and tissue research. Springer, Berlin, pp 371–391

Kroon M, Holzapfel GA (2008a) Elastic properties of anisotropic vascular membranes examined by inverse analysis. Comput Methods Appl Mech Engrg 198:3622–3632

Kroon M, Holzapfel GA (2008b) Estimation of the distributions of anisotropic, elastic properties and wall stresses of saccular cerebral aneurysms by inverse analysis. Proc R Soc 464:807–825

Kroon M, Holzapfel GA (2009) A theoretical model for fibroblast-controlled growth of saccular cerebral aneurysms. J Theor Biol 257(1):73–83

Lagarias JC, Reeds JA, Wright MH, Wright PE (1998) Convergence properties of the nelder-mead simplex method in low dimensions. SIAM J Optim 9(1):112–147

Lu J, Zhou X, Raghavan ML (2007) Inverse elastostatic stress analysis in pre-deformed biological structures: demonstration using abdominal aortic aneurysms. J Biomech 40:693–696

Lu J, Zhou X, Raghavan ML (2008) Inverse method of stress analysis for cerebral aneurysms. Biomech Model Mechanobiol 7:477–486

Menashi S, Campa JS, Greenhalgh RM, Powell JT (1987) Collagen in abdominal aortic aneurysm: typing, content, and degradation. J Vasc Surg 6:578–582

Nelder JA, Mead R (1965) A simplex-method for function minimization. Comput J 7(4):308–313

Raghavan ML, Vorp DA, Federle M, Makaroun MS, Webster MW (2000) Wall stress distribution on three dimensionally reconstructed models of human abdominal aortic aneurysm. J Vasc Surg 31:760–769

Raghavan ML, Ma B, Fillinger MF (2006) Non-invasive determination of zero-pressure geometry of arterial aneurysms. Ann Biomed Eng 34(9):1414–1419

Rissland P, Alemu Y, Einav S, Ricotta J, Bluestein D (2009) Abdominal aortic aneurysm risk of rupture: patient-specific fsi simulations using anisotropic model. J Biomech Eng 131:031,001

Sheidaei A, Hunley SC, Zeinali-Davarani S, Raguin LG, Baek S (2010) Simulation of abdominal aortic aneurysm growth with updating hemodynamic loads using a realistic geometry. Med Eng Phys (in print). doi:10.1016/j.medengphy.2010.09.012

Speelman L, Bohra A, Boosman EMH, Schurink GHW, van de Vosse FN, Makaroun MS, Vorp DA (2007) Effects of wall calcifications in patient-specific wall stress analyses of abdominal aortic aneurysms. J Biomech Eng 129(1):105–109

Taylor CA, Humphrey JD (2009) Open problems in computational vascular biomechanics: hemodynamics and arterial wall mechanics. Comput Methods Appl Mech Eng 198:3514–3523

Torczon VJ (1989) Multi-directional search: a direct search algorithm for parallel machines. PhD thesis, Rice University

Vande Geest JP, Sacks MS, Vorp DA (2004) Age dependency of the biaxial biomechanical behavior of human abdominal aorta. J Biomech Eng 126:815–822

Vande Geest JP, Sacks MS, Vorp DA (2006) The effects of aneurysm on the biaxial mechanical behavior of human abdominal aorta. J Biomech 39:1324–1334

Vorp DA, Vande Geest JP (2005) Biomechanical determinants of abdominal aortic aneurysm rupture. Arterioscler Thromb Vasc Biol 25(8):1558–1566

Watton PN, Hill NA (2009) Evolving mechanical properties of a model of abdominal aortic aneurysm. Biomech Model Mechanobiol 8(1):25–42

Wright MH (1996) Direct search methods: once scorned, now respectable. In: Griffiths DF, Watson GA (eds) Numerical analysis 1995. Addison-Wesley, Reading, pp 191–208

Zeinali-Davarani S, Choi J, Baek S (2009) On parameter estimation for biaxial mechanical behavior of arteries. J Biomech 42(4):524–530

Zeinali-Davarani S, Sheidaei A, Baek S (2010) A finite element model of stress-mediated vascular adaptation: application to abdominal aortic aneurysms. Comput Methods Biomech Biomed Eng (in print). doi:10.1080/10255842.2010.495344

Zhou X, Lu J (2009) Estimation of vascular open configuration using finite element inverse elastostatic method. Eng Comput 25:49–59

Zhou X, Raghavan ML, Harbaugh RE, Lu J (2010) Specific wall stress analysis in cerebral aneurysms using inverse shell model. Ann Biomed Eng 38(2):478–489